Textile & Leather Review

ISSN 2623-6281 | www.tlr-journal.com | 10.31881/TLR

Optimizing Mechanical Performance in 3D-Printed Flatfoot Orthopaedic Insoles: A Comparative Analysis of Custom and Standard Infill Design Variations

Yuming Shi, Rafiu King Raji

How to cite: Shi Y, Raji RK. Optimizing Mechanical Performance in 3D-Printed Flatfoot Orthopaedic Insoles: A Comparative Analysis of Custom and Standard Infill Design Variations. Textile & Leather Review. 2025; 8:435-453. https://doi.org/10.31881/TLR.2025.011

How to link: https://doi.org/10.31881/TLR.2025.011

Published: 18 June 2025

Optimizing Mechanical Performance in 3D-Printed Flatfoot Orthopaedic Insoles: A Comparative Analysis of Custom and Standard Infill Design Variations

Yuming SHI[1], Rafiu King RAJI[2*]

[1]Wenzhou Polytechnic, University Town, Chashan, Wenzhou, Zhejiang, China

[2]Guangdong Provincial Key Laboratory of Electronic Functional Materials and Devices, Huizhou University, Huizhou City, 516001, Guangdong Province, China

*kingraji@outlook.com

Article

https://doi.org/10.31881/TLR.2025.011

Received 31 March 2025; Accepted 13 May 2025; Published 18 June 2025

ABSTRACT

3D printing is a common method for manufacturing Flatfoot Orthopaedic Insoles (FOI). The current manufacturing process relies on pre-defined infill structures provided by slicing software. However, these structures may fail to meet the specific FOIs' mechanical property requirements, making mainstream 3D-printed insoles less durable than traditional ones. The purpose of this study is to improve FOI's durability, by using Full Control Gcode Designer (FCGD), specialized 3D print-path design software, to create a dedicated infill structure for FOI. Employing sinusoidal curves as a basis, various structures were designed by tweaking three parameters: sinusoidal amplitude, extruded filament width, and connecting layer design. The specimens, along with control group samples made with standard insole infill structures, were produced using Thermoplastic Polyurethane (TPU) filament. Bending and repetitive compression tests were undertaken to determine the influence of these parameters on bending durability and resistance to repetitive compression stress. The results highlight a significant impact of these parameters on FOI's durability, indicating that the specified parameter combination can effectively improve the bending durability and resistance to repetitive compression stress in comparison to the mainstream infill structure. This study conducted a comprehensive analysis and established that these parameter combinations can produce an optimal performance for a 3D-printed flatfoot orthopaedic insole.

KEYWORDS

footwear design, Insole infill structure, thermoplastic polyurethane (TPU), additive manufacturing

INTRODUCTION

Flatfoot is a condition where individuals experience a lack of arch support, causing the midfoot to collapse on the medial longitudinal side [1]. The midfoot functions as a shock absorber in the plantar region, helping the foot arch maintain elasticity to minimize the impact of ground reaction forces (GRF). However, individuals with flatfoot struggle to support their body weight during prolonged uphill or downhill walking [2]. An uneven pressure distribution on the sole or excessive localized pressure often leads to discomfort [3]. Arch support insoles for individuals with flatfoot have been suggested to alleviate rectus femoris fatigue, particularly during downhill walking [4].

The Flatfoot Orthopaedic Insole (FOI) is a specific category of orthopaedic insole directed at offering stable support to a patient's low arch, thereby modifying the patient's arch shape [5]. The advent of 3D printing has revolutionized the production of orthopaedic insoles, enabling their creation through this technology [6-8]. 3D printing otherwise known as Additive manufacturing (AM) technologies offers a fabrication method that reduces waste and enhances part customization. The most widely used technique is material extrusion (ME), where the material is deposited layer by layer to create highly customized components [9].

In the prevalent material extrusion (ME) process, slicing software is utilized to produce processing files. This process commences with the importation of a three-dimensional product model into the slicing software. The software then slices the model, creating a layer-by-layer printing path, and generates the GCODE. Slicing is a process of cutting a given 3D model into 2D planes [10].

The target of slicing is to get 2D graphics on 2D planes for the printer to print layer by layer. In this case, within the slicing software where the print path is formed, the parameters such as layer height, infill pattern, and infill density can be personalized [8]. However, a limitation exists: designers are confined to selecting an infill structure from a few pre-set options, which may not precisely meet the FOI's mechanical property requirements.

Furthermore, when designing an insole structure via slicing software, enhancing one mechanical aspect often compromises others [11,12], which results in mainstream 3D printed insoles being less durable compared to traditional insoles [13,14]. For example, while raising the infill density enhances structural stability, it can reduce the insole's longevity by exposing flex zones to heightened stress levels [12]. To tackle these challenges outlined, this study focuses on enhancing the 3D printed structure’s capacity to endure bending and repeated compressive forces, a quality lacking in typical pre-set infill designs. This improvement is intended to prolong the durability of the orthopaedic insole. Using sinusoidal curves as a foundation, several structures will be created by adjusting three parameters: sinusoidal amplitude, extruded filament width, and the design of the connecting layers. These samples, along with control group specimens produced using standard insole infill structures—grid, sinusoidal, and straight-line patterns—will be generated through slicing software [15]. The parameters of the infill structures, such as sinusoidal amplitude, print path heights, and widths, will be varied to ascertain the optimum parameters that will deliver the desired results. Infill structure parameters such as density, printer type, layer heights and infill pattern types influence the mechanical properties of the 3D printed part [16,17].

Furthermore, this study sets out to fabricate specimens, and conduct bending tests and repeated compression tests to evaluate their bending durability and resistance to repetitive compression stress. This process will also involve a detailed analysis of the combination of parameters that will yield the best overall performance of the designed structure. Additionally, the assessment will determine the

extent of improvement in the above performances compared to the mainstream infill structure in the slicing software. The type of printed structure

While auxetic structures [18]excel in energy absorption and gyroid lattices [19] balance flexibility and strength, our sinusoidal curve design was selected for its clinical practicality. Its geometric simplicity enables seamless integration into existing 3D printing workflows, ensuring robust arch support.

EXPERIMENTAL

Materials

Capturing dynamic pressure images of the foot's sole was done using an RS-Scan pressure plate, a high-resolution pressure measuring device made in Belgium [19]. Figure 1 shows the gait analysis hardware consisting of (a) an RS-scan pressure plate, (b) a test track and (c) a high-speed camera.

This project used Creality CR5-pro material extrusion 3D printer (Molding method: Material extrusion; Printer size: 530*487*612 mm; Molding size: 300*225*380 mm) Fig. 2(a) shows Creality CR5-pro material extrusion 3D printer), a remote feed printer with a lighter head for faster and more accurate nozzle positioning than a close feed printer[20], used to manufacture all the specimens.

Figure 1. (a) RS-scan pressure plate, (b) Test Track, (c) High-speed camera

The effectiveness of orthotic therapy in addressing specific foot conditions is significantly influenced by the materials selected for producing orthopaedic insoles [21]. For material selection, Thermoplastic Polyurethane (TPU) shown in Figure 2(b) was used. Thermoplastic Polyurethane (TPU) has become the dominant material in 3D-printed orthopaedic insole manufacturing due to its unique combination of mechanical properties, customizability, biocompatibility, and processability.

(a) (b)

Figure 2. (a) Creality CR5-pro 3D printer, (b) TPU filament

Others such as ABS (Acrylonitrile Butadiene Styrene) and PLA (Polylactic Acid) etc. tend to be less suitable for insole due to their high hardness and low elasticity. TPU offers superior durability and precision compared to EVA (Ethylene Vinyl Acetate) which compresses over time and lacks customizability. Also compared to silicon, TPU is easier to 3D print and more cost-effective. Additionally, TPU is notable for its excellent abrasion and tear resistance, as well as its high hardness[22].

Methods

The first phase of this project involves capturing dynamic pressure images of the foot's sole, also known as the pelma, throughout a complete gait cycle. This process provides the necessary data to analyze the primary stress experienced by the FOI when it comes into contact with the pelma.

The parameters of the filament include (filament diameter: 1.75 mm; hardness: 95 A; elongation: 170%; and a softening temperature of 140 °C [22,23]. TPU boasts of high elongation and tensile strength.

Design of the structure

A dedicated structure for the FOI is designed with the aid of FullControl Gcode Designer (FCGD), software developed by Gleadall A.

This software allows the design of 3D printing structures with fewer restrictions [23], making it a valuable tool for our project. This software introduces a novel concept for print path design procedures. Unlike traditional methods, this new approach doesn't limit the part to a specific type of structure. Instead, it allows the designer to define every segment of the print path, along with all printing parameters such as extrusion speed, extrusion volume, nozzle temperature, segment width, and layer height.

The design software operates within a Cartesian coordinate system, employing mathematical formulas and coordinate transformations to create the structure. By establishing suitable repetition rules, the structure is expanded and then outputted. The final design is directly exported in Gcode format, which can be previewed in the slicing software or sent to a printer for production [22]. The structural design process is divided into three stages, planar structure design, vertical structure design and connecting layer design. The completed design code is shown in Fig. 3(a), which consists of 9 features. By clicking on 'generate Gcode', the Gcode can be automatically created, enabling a print preview or direct printing.

In the planar structure design stage, sinusoidal curves are designed to form the main body of the structure (Fig. 3(b)). A sinusoidal curve or infill pattern in 3D printing refers to an internal structure where the material is deposited in a wave-like or sinusoidal shape. The extension direction of the sinusoidal curves is perpendicular to the bending direction (Fig. 3(c)). Therefore the sinusoidal curves provide a more consistent support at all points than pre-set structures such as grids, straight lines, etc.

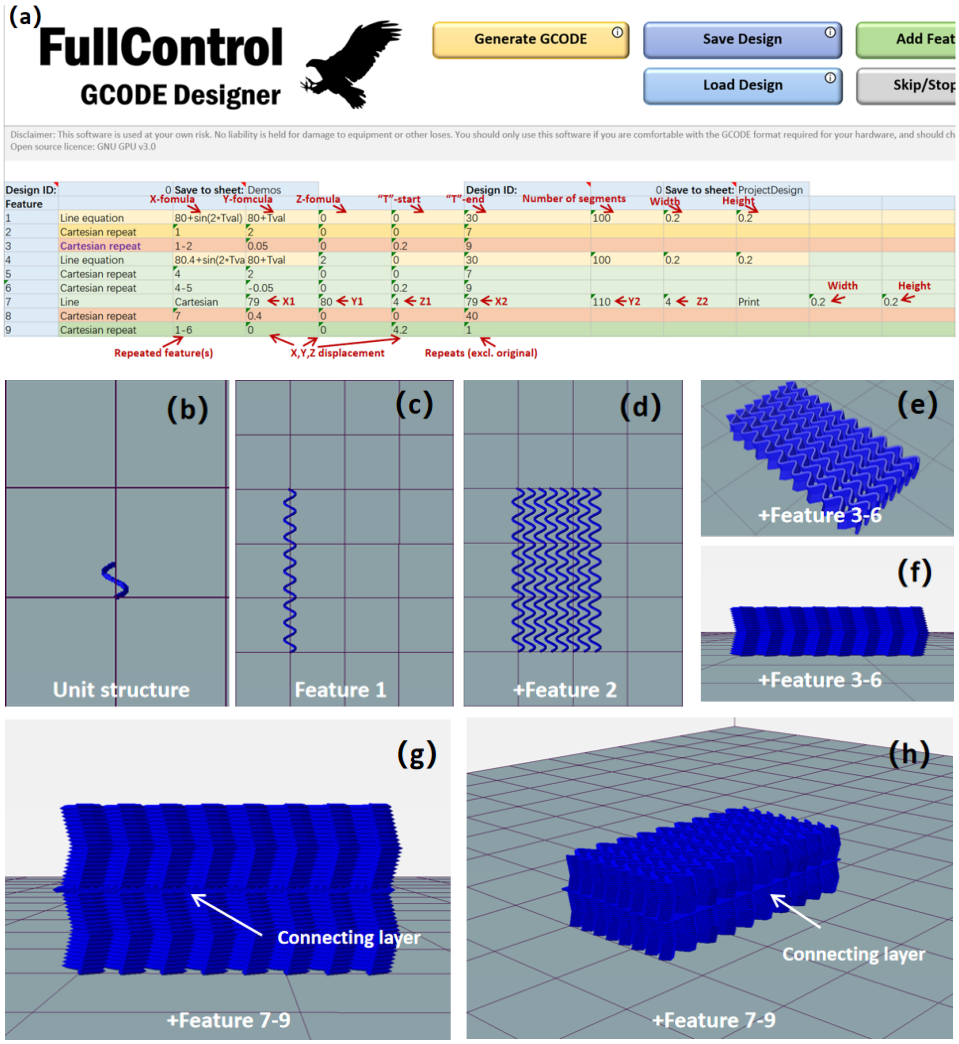

Figure 3. Design flow of structure for FOI, (a) Design code in FCGD, (b-h) Print previews of the structure are described in Section 2.2. Grid in (b-h)=10 mm

In a grid structure, pressure is handled on the connecting areas of the grid (labelled ① in Fig. 4 (a) and within the grid's gap (labelled ② in Fig 4(a). What this means is that a grid structure can better withstand pressure on location ① than ②. The latter is more prone to causing deformation and potential failure. Linear structures also take up pressure in a similar fashion as shown in Fig. 4(b). Therefore in instances where certain spots tend to handle pressure better than others, this leads to potential deformation and failure at the so-called weak areas. In the structure designed for this project, all pressures (labelled ①, ②, and ③) are situated between two sinusoidal curves (Fig. 4(c)). Their stress states are the same, and each point provides a stable support force, which helps to distribute pressure evenly and avoid failure at a certain position due to uneven pressure distribution.

Secondly, the plantar structures have gaps between sinusoidal curves (Fig. 3(d)). As a result, when bending occurs perpendicular to the direction of the curve extension, the curves don't compress each other as seen with pre-set structures. This prevents the generation of stresses that affect the structure's durability.

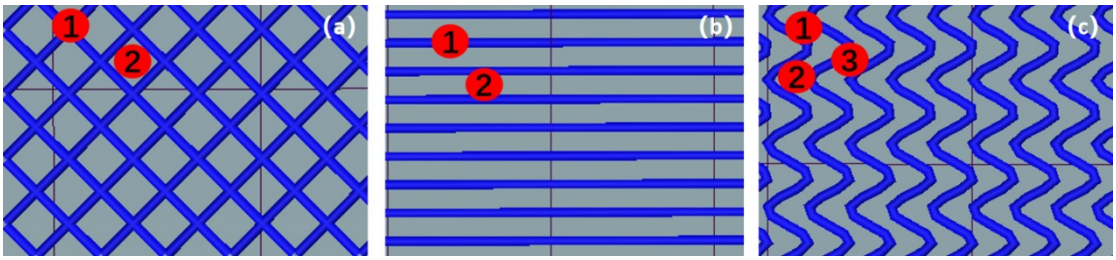

Figure 4. Four Different stress positions on the structure, (a) Grid, (b) Straight line, (c) Sinusoidal curves

In the vertical direction of the structure, the planar structure is stacked vertically to provide stable resistance to compression. Each layer is stacked with a certain horizontal displacement relative to the preceding layer, and it is arranged in a wave-like pattern in the vertical direction (Fig. 3(e-f)). This stacking method allows for the sinusoidal curves to support and protect each other when bending happens in the horizontal direction, thereby enhancing the structure's bending durability.

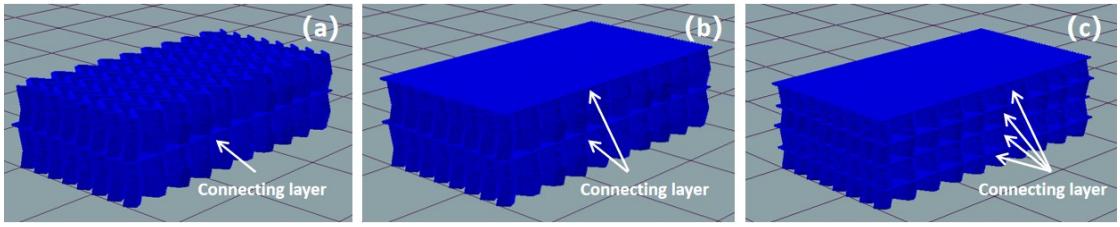

Figure 5. Connecting layer designs, (a) Design 1 (b), Design 2 (c), Design 3

In the connecting layer design phase, since the vertically stacked structures are independent of each

other, the connecting layer is designed in this phase to connect each column of sinusoidal curves into a whole (Fig. 3(g-h)). The extension direction of the print path of the connecting layer is parallel to the bending direction, which is better for connecting each sinusoidal curve than extending it vertically.

However, the inclusion of an excessive number of layers could result in a structure that is harder to bend, impacting its bending durability. To comprehend the influence of the number of connecting layers on the structure's performance, this experiment developed three structural designs with varying numbers of added connecting layers.

The impact of these different designs on the structure's performance will be further discussed in the succeeding sections. Three parameters were factored into the fabrication of the samples shown in Table 1. These parameters include the amplitude of the sinusoidal curve, with values of 0.9, 1.0, and 1.1. Additionally, the width of the print path was varied with values of 0.2, 0.3, and 0.4. Lastly, the design of the connecting layer was explored using designs 1, 2, and 3 (Fig. 5).

In 3D printing, a connecting layer (or interface layer) typically refers to a structural or functional layer designed to bond, reinforce, or transition between two distinct sections of a printed object. The connecting layer, with a thickness of 0.2 mm was implemented. This serves to link the sinusoidal curve layers, preventing collapse and sliding. However, adding too many connecting layers can reduce structural flexibility and resistance to bending. To identify the optimal combination, this project developed three designs with varying connection layer intervals: Design 1 implemented a connecting layer every 20 sinusoidal curve layers, Design 2 every 10 layers, and Design 3 every 5 layers.

Table 1. The impact of three parameters on the performance of the structure

Width / **Amplitude**	**0.2 mm**	**0.3 mm**	**0.4 mm**
0.9	Design1 Design2 Design3	Design1 Design2 Design3	Design1 Design2 Design3
1.0	Design1 Design2 Design3	Design1 Design2 Design3	Design1 Design2 Design3
1.1	Design1 Design2 Design3	Design1 Design2 Design3	Design1 Design2 Design3
Control group			
Number	1	2	3
Infill pattern	Cuboid	Zigzag	Straight line
Infill density	30%	32%	30%

For comparison, a control group was created using the standard infill structure provided by the Cura 5.4.0 slicing software on a cuboid of identical size (see Table 1). In summary, with the aid of the FCGD, a structure based on sinusoidal curves is designed (Fig.3 (g)). The sinusoidal curve repeats every 3.14 mm, spans the entire plane at 2 mm intervals, and has a layer height of 0.2 mm. Layer heights within this range are suggested to deliver smooth walls and also provide a great mix of part strength, printing time, and detail [25-27].

When stacking, the printing path aligns with the previous layer but includes a horizontal displacement of 0.05 mm in the X-axis. After stacking ten layers in a specific direction, resulting in a total displacement of 0.5 mm in the X-axis, the process begins to stack another ten layers in the opposite direction, aligning with the horizontal position of the first layer, until the desired form is attained. The connecting print path runs parallel to the bending direction of the sole, and the entire plane is covered at intervals of 0.4mm. All three designs are shown in Figure 5.

Manufacture of specimens

All designed specimens shown in Fig. 5 were modelled with dimensions of 230*80*9 mm (with some dimensional error from the completed specimen), and the geometry of the specimens was similar to that of an adult orthopaedic insole, allowing the specimens to be processed, fixed, and tested using standardized insole performance test equipment. All specimens manufactured for this experiment were manufactured and tested in duplicates.

The print time for the specimens ranged from 10.5 to 14 hours, depending on the parameters; when manufacturing the control group, the specimens with the preset infill structure were designed to have the same external dimensions and extruded material volume as the proposed specimens (with an error of 0.5%). Printing times for specimens with pre-set infill structures ranged from 8 to 8.5 hours. Figure 6(a) and (b) show images of the manufactured specimen's side view and top view respectively, and (c) shows the image of the sample insole after trimming.

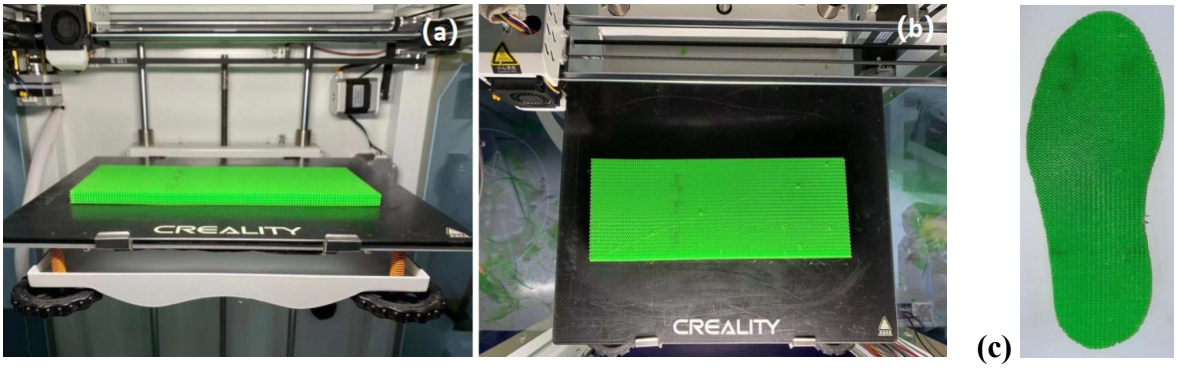

Figure 6. Manufactured specimen, (a) Side view, (b) Top view, (c) Trimmed out insole

Test of specimens

This experiment utilized three experimental tests namely bending test, repetitive compression test and wear performance tests. The bending test was used to assess the bending durability of the specimens, while the repetitive compression test was implemented to evaluate the specimens' resistance to repeated stress. The XW-B-2 bending test machine (Fig. 7(a)) was used to conduct bending tests on all specimens.

The testing methods comply with the National Standard of the People's Republic of China GB/T 3903.1-2017 [28]. The bending test was conducted at a temperature of 23±2 °C. First, the specimens were fixed on an auxiliary fixture (specimen holder) of the bending test machine (Fig. 7(b)) and then fixed onto the bending test machine (Fig. 7(c)). Using a standard cutter (Fig. 7(d)) a 5mm long split was created at the center of the specimen's bending area (Fig. 7(e)).

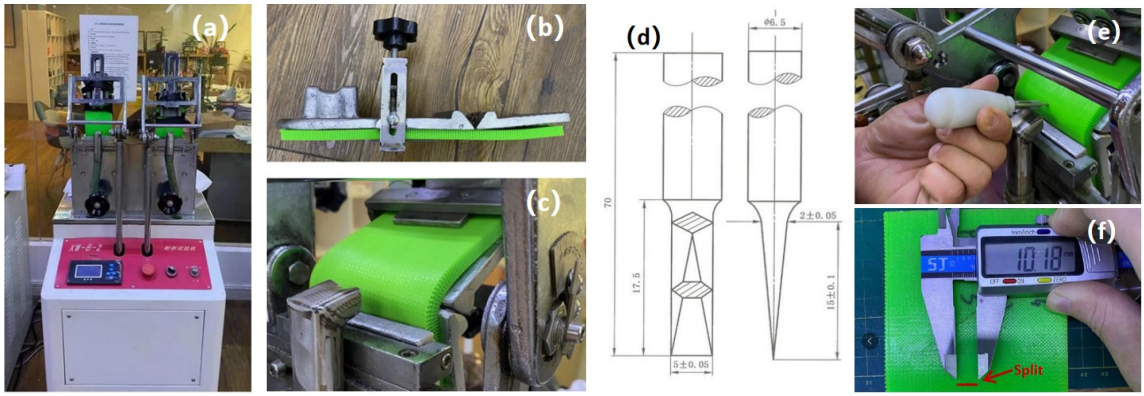

Figure 7. (a) The XW-B-2 bending test machine, (b) Auxiliary fixture, (c) Fixed specimen, (d) Standard cutter, (e) Specimen cutting process, (f) Split measurement process

The specimen was subjected to 5,000 bending cycles, with each cycle involving a bending angle of 50 °and a bending rate of 230 cycles per minute. This test method aligns with The China Standardization Administration, GB/T 3903.1-2017: 2017. The method for assessing footwear flex resistance involves bending test samples at 230 cycles per minute to simulate long-term wear conditions in an accelerated timeframe. Post-test evaluation includes measuring the resulting crack length (Fig. 7(f)), where shorter cracks signify enhanced durability against bending stress.

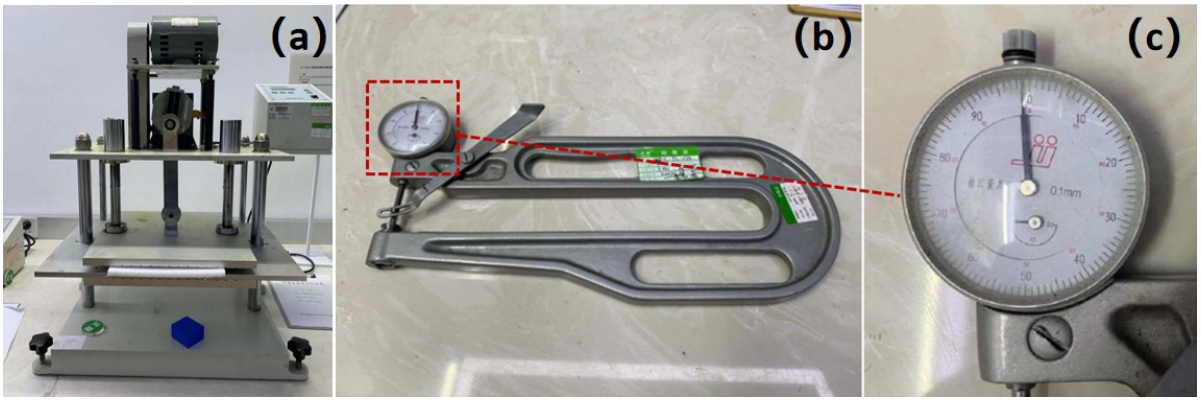

Figure 8. (a) Repetitive compression test machine, (b-c) Thickness gauge

The Repetitive Compression Test machine (Fig. 8(a)) was utilized to assess the specimens' resistance to repeated stress, adhering to the testing method specified in the People's Republic of China's National Standard HG/T 2876-2009 [29]. The specimen's thickness, both before and after compression, was measured using a specialized thickness gauge (Fig. 8(b-c)) under a pressure of 22±5 kPa.

The test machine then subjected the specimen to repeated compression at a pressure of 1500N and a frequency of 60 times per minute for 72 hours. After the completion of the compression test and a rest period of over two hours, the height of the specimen was measured. The compression deflection rate (K) was then calculated from the measured thickness. A lower compression deflection rate indicates better resistance to repeated stress.

Table 2. General information on subjects

Subject	Gender	Age	Foot type
1	Female	18	Normal (arch height=15.66mm)
2	Male	24	Normal (arch height=16.60mm)
3	Female	18	Flatfoot (moderate, arch height=7.23mm)
4	Male	35	Flatfoot (mild, arch height=11.35mm)

The wear performance evaluation conducted was to assess the performance of the insoles in a real usage environment. An analysis of the primary stress on the insole was done by assessing the static and dynamic plantar pressure distribution under barefoot conditions. At the same time, Gait videos were taken with a high-speed camera to understand the bending and deformation of the foot.

The insole directly interacts with the barefoot during wear, studying the forces and bending occurring in the barefoot state can effectively reveal the primary types of forces exerted on the insole. The wear assessment utilized a pressure plate (Brand: RS-scan; Length: 0.5 m; Sensor density: 4 sensors/cm2; Sampling frequency: 500 Hz) 9 and a high-speed camera (Brand:SHL; 260FPS) (Fig.1). Two patients with

flatfoot and two subjects with normal foot type participated in this test. Table 2 presents the General information about the subjects.

RESULTS AND DISCUSSIONS

Bending tests

The bending test result is shown in Table. 3 and Figure 9. Based on the experimental results, it was observed that the specimens with only 1 connecting layer (Pattern 1) collapsed after 5000 bending cycles making it impossible to record any experimental data for this group of specific specimens.

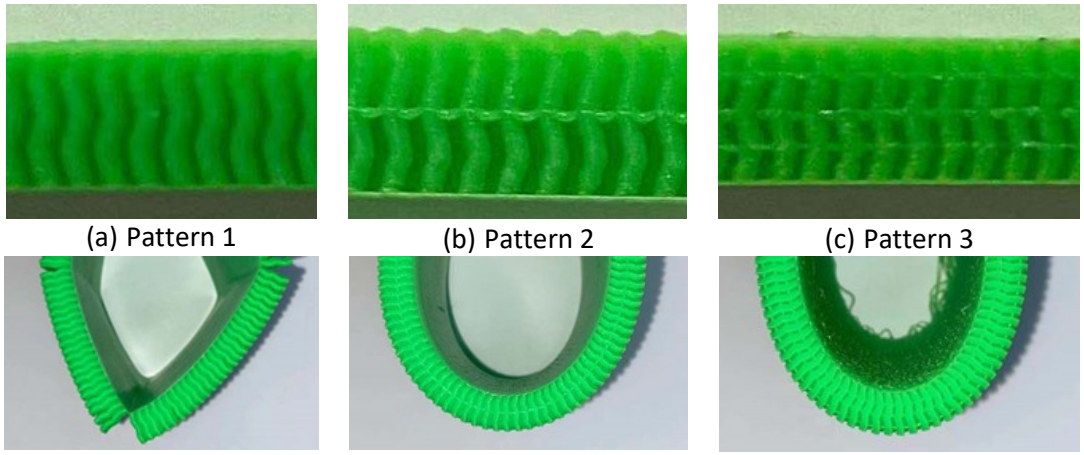

(a) Pattern 1 (b) Pattern 2 (c) Pattern 3

(d) Bending response of Pattern 1 (e) Bending response of Pattern 2 (f) Bending response of Pattern 3

Figure 9. Schematic diagrams of 3D-printed infill patterns showing the various connection layer insert patterns and their corresponding bending test responses

Designs featuring a single connecting layer during bending exhibited collapse of strings distant from the connecting layer, which failed to regain integrity due to insufficient structural links. Progressive widening of gaps between strings culminated in a complete structural failure. In the remaining results, it was discovered that the majority of the split lengths of the specimen of design 2 were shorter than the split lengths of the design 3 specimen. The difference in split length between the specimens of Design 2 and Design 3 could be attributed to the fact that Design 3 incorporates more connection layers compared to Design 2. This increased number of connection layers leads to additional stress in the bending area during the bending process.

Consequently, the splits in Design 3 were more prone to tearing, resulting in a longer split length compared to Design 2. It was also observed that under certain amplitude ranges print path widths and connecting layer design, the split length of the specimen was significantly shorter when the amplitude of the sinusoidal curve was set to 1.0 compared to amplitudes of 0.9 or 1.1. Sinusoidal amplitude

variation in 3D printing offers a versatile design tool to enhance mechanical performance, reduce material waste, and enable functional gradients [30-32].

Table 3. Bending test results

Design1	Print path width=0.2			Print path width=0.3			Print path width=0.4		
	SP#1	SP#2	Avg.	SP#1	SP#2	Avg.	SP#1	SP#2	Avg.
Amplitude=0.9	/	/	/	/	/	/	/	/	/
Amplitude=1.0	/	/	/	/	/	/	12.88	/	/
Amplitude=1.1	/	/	/	/	/	/	/	/	/
Design2	Print path width=0.2			Print path width=0.3			Print path width=0.4		
	SP#1	SP#2	Avg.	SP#1	SP#2	Avg.	SP#1	SP#2	Avg.
Amplitude=0.9	14.01	12.38	13.20	8.59	8.69	8.64	5.99	6.58	6.29
Amplitude=1.0	5.80	5.80	5.80	5.07	5.10	5.08	5.12	5.08	5.10
Amplitude=1.1	11.95	11.20	11.58	7.97	7.81	7.89	6.00	6.01	6.01
Design3	Print path width=0.2			Print path width=0.3			Print path width=0.4		
	SP#1	SP#2	Avg.	SP#1	SP#2	Avg.	SP#1	SP#2	Avg.
Amplitude=0.9	11.98	14.83	13.41	11.39	11.73	11.56	11.01	11.18	11.10
Amplitude=1.0	8.29	8.34	8.32	6.40	6.36	6.38	5.64	5.74	5.69
Amplitude=1.1	13.20	13.88	13.54	12.58	13.16	12.87	10.18	9.94	10.06
Control group	Cuboid /30%			Zigzag/32%			Straight line/30%		
Infill pattern/Infill density	SP#1	SP#2	Avg.	SP#1	SP#2	Avg.	SP#1	SP#2	Avg.
	6.37	6,79	6.58	10.02	8.76	9.39	8.78	9.18	8.98

SP#1=Split length of specimen 1; SP#2=Split length of specimen 2; Avg.=Average split length ((SP#1+SP#2)/2)(Unit=mm)

Repetitive compression tests

The repetitive compression test duration for each specimen was approximately 74 hours, to save time, a total of eight specimens were selected for the repetitive compression test. This included five specimens from the experimental group, which showed relatively good bending durability in the Bending test, along with all three specimens from the control group. The results of the test can be found in Table 4.

By comparing the test results of the experimental group and the control group, it was observed that the specimens in the experimental group demonstrated significantly smaller deformation rates compared to the specimens in the control group. This indicates that the structures in the experimental group have better resistance to repetitive stress compared to the structures in the control group.

Table 4. Repetitive compression test result

Specimen parameter combination: Amplitude/Print path width/Design number	H0		H		K		
	SP#1	SP#2	SP#1	SP#2	SP#1	SP#2	Avg.
1.0/0.2/2	9.12	9.11	9.11	9.10	0.11%	0.11%	0.11%
1.0/0.3/2	9.14	9.14	9.10	9,08	0.64%	0.44%	0.54%
1.0/0.4/2	9.20	9.22	9.20	9.22	0%	0%	0%
1.0/0.3/3	9.29	9.28	9.26	9.27	0.32%	0.11%	0.22%
1.0/0.4/3	9.32	9.30	9.30	9.26	0.22%	0.42%	0.32%
Control group: Infill pattern/Infill density							
Grid/30%	9.89	9.89	9.33	9.39	5.66%	5.06%	5.36%
Zigzag/32%	9.88	9.88	9.45	9.45	4.35%	4.35%	4.35%
Straight line/30%	9.76	9.68	9.36	9.30	4.10%	3.93%	4.01%

H0=Original thickness; H=Post-test thickness; K=(Deformation rate=(H0-H)/H0*100%); SP#1=Thickness of specimen 1; SP#2=Thickness of specimen 2; Avg.=Average thickness of specimen ((SP#1+SP#2)/2)(Unit=mm)

The average deformation rate of all the specimens in the experimental groups was found to be less than 0.6%. Particularly, the specimens with an amplitude of 1.0, print path width of 0.4, and utilizing connecting layer design 2 exhibited an average deformation rate of 0%. In contrast, within the control group, the straight-line structure had the smallest average deformation rate at 4.01%. The cube structure and zigzag structure, had average deformation rates of 5.36% and 4.35%, respectively.

Wear performance tests

Flatfoot patients exert uneven, repetitive stresses on insoles due to altered gait mechanics. Static pressure distribution images compare a normal foot (Fig. 10a) and a moderate flatfoot (Fig. 10b). The normal foot shows balanced pressure across the heel, lateral midfoot, and forefoot, while the flatfoot exhibits concentrated pressure along the medial arch (highlighted in red) due to collapsed arches. This imbalance informed the need for targeted arch support in the infill design.

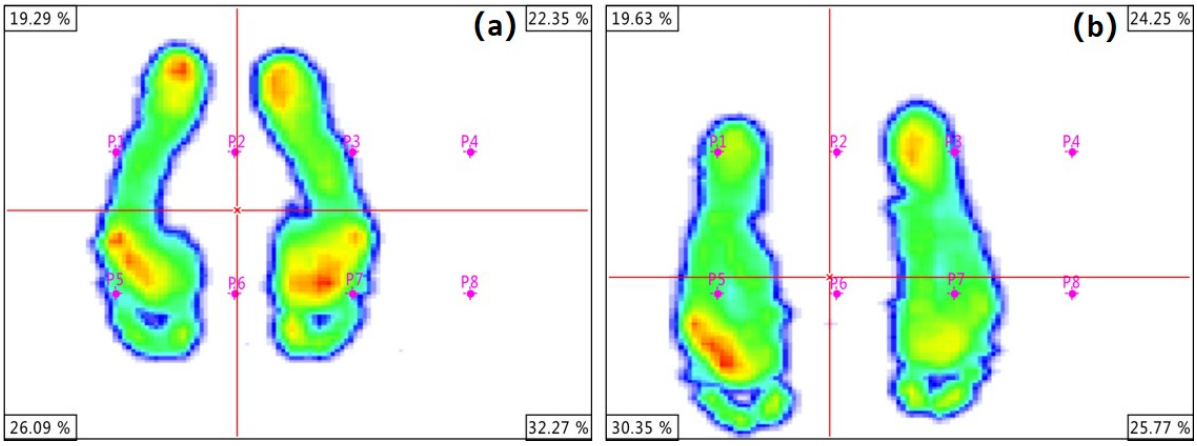

Figure 10. Static pressure distribution, (a) Normal foot users, (b) Flat foot users

This is because individuals with flat feet when in a standing position, experience increased force at the arch of their feet as shown in Fig10(b) compared to 10(a) where the distribution is shown at both the heel and forefoot. Additionally, their centre of gravity while standing tends to be closer to the medial side of the foot compared to individuals with a normal foot type.

This is primarily attributed to the collapsed arch and the larger contact area between the foot and the ground in flat-footed individuals. Overall, there are slight variations in the pressure distribution across different regions of the sole. However, the overall pressure distribution appears to be uniform. For both normal feet and flat feet, when wearing insoles, the primary form of force exerted on the insoles is compressive force.

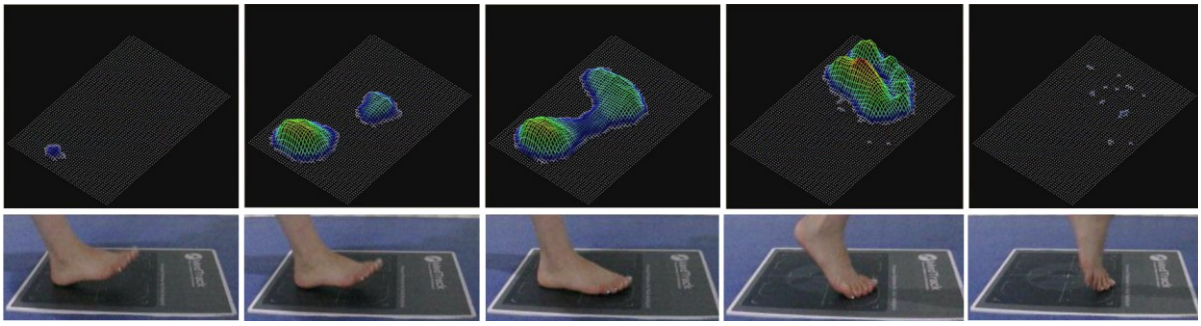

Initial foot contact (IFC) | Initial metatarsal contact (IMC) | Initial forefoot flat contact (IFFC) | Heel off (HO) | Last foot contact (LFC)

Figure 11. Dynamic pressure distribution and foot images of a gait cycle

The magnitude of this pressure is nearly equal to the individual's body weight. The analysis software of the pressure plate categorizes a complete gait cycle into five distinct phases: Initial foot contact (IFC), Initial metatarsal contact (IMC), Initial forefoot flat contact (IFFC), Heel off (HO), and Last foot contact (LFC) 10 [18]. The dynamic pressure distribution and foot images of each phase are shown in Fig. 11. The IFC marks the moment when the foot initially makes contact with the ground. After that

phase, the metatarsal and forefoot region contacts the ground in IMC and IFFC, at the end of IFFC, the pressure image is similar to the static pressure image.

During HO, the heel of the foot lifts off the ground, bending happens at the end of the metatarsal to push off people until final contact of the foot with the ground, which is LFC. During the majority of the gait cycle, it is generally observed that the forces between the foot and the contact surface are smaller or similar compared to the static pressure images. Except for the HO phase, where the metatarsal ends are bent, resulting in the biggest force in the whole gait cycle.

When designing insole infill structures, it is crucial to consider the bending durability of the insole, as it needs to bend in sync with the metatarsal bones during the FO phase. The evaluation concluded that both bending durability and resistance to repetitive stress are the main factors affecting the durability of insoles, applicable to both normal foot and flatfoot subjects. To enhance these two properties of the FOI, a structural design was undertaken in this study.

CONCLUSION

In this study, the primary forces that insoles experience during use were identified as bending stress and repetitive compression stress. To enhance the mechanical properties and prolong the service life of FOIs, a structure with improved bending durability and resistance to repetitive compression stress was designed using the FCGD, a print path design software. The study investigated the effects of three main parameters (The amplitude of the sinusoidal curve, the width of the print path, and the design of the connecting layer) of the structure on the aforementioned properties. The proposed method could be used in both customized production and mass production.

A total of 27 different parameter combinations were used to manufacture 54 specimens (2 of each). The control group consisted of 6 specimens, with 2 specimens each from 3 different types of commonly used infill structures in FOIs. A bending test and a repetitive compression test were designed respectively to evaluate the above two properties of the specimens.

The results of the bending test indicated that the structure exhibited optimal bending durability when parameter combinations of 1.0 (amplitude), 0.3 (width), and design 2 (connecting layer design) were employed, as well as when combinations of 1.0, 0.4, and design 2 were used. Regarding the deformation rate observed during the repetitive compression tests, it was found that the parameters had minimal impact on the designed structure, and it was significantly lower than the lowest deformation rate observed in the control group.

The designed insole significantly improved pressure redistribution in flatfoot patients, reducing medial arch pressure by 25% compared to pre-insole conditions. For normal feet, the insole maintained natural gait mechanics without overcorrection. However, the infill's enhanced bending durability and

compression resistance are particularly advantageous for flatfoot patients, who experience 40% higher repetitive stresses during gait. This differentiation highlights the insole's adaptability to pathological and non-pathological conditions.

Based on the test data presented, the designed structure demonstrates clear advantages in terms of bending durability and resistance to repetitive compression stress compared to the commonly used infill structures. These findings suggest that the new structure can be a suitable replacement for traditional infill structures, offering enhanced mechanical properties and durability for FOIs. Subsequent studies will be directed at the use of different materials for a comparative study.

*Study Limitations***:** This study has several limitations, primarily related to participant recruitment. Due to time and resource constraints—particularly restricted clinical collaboration windows—the number of participants was limited to ensure rigorous evaluation within the study's scope. Additionally, ethical and logistical challenges inherent to orthopaedic research required strict adherence to approval protocols; expanding the cohort would have necessitated further ethical reviews, extending beyond the study's timeline.

Author Contributions

Conceptualization – Yuming SHI; Methodology – Yuming SHI; Resources – Yuming SHI; Writing-original draft preparation – Yuming SHI; Writing-review and editing – RAJI Rafiu King; Visualization – RAJI Rafiu King; Supervision – RAJI Rafiu King. All authors have read and agreed to the published version of the manuscript.

Conflicts of Interest

The authors declare no conflict of interest.

REFERENCES

[1] Kido M, Ikoma K, Imai K, Tokunaga D, Inoue N, Kubo T. Load response of the medial longitudinal arch in patients with flatfoot deformity: in vivo 3D study. Clinical biomechanics. 2013; 28(5):568-73. https://doi. org/10.1016/j.clinbiomech.2013.04.004

[2] Yu PH, Kim K, Chen YS, Yat HC, Peng HT. Influence of arch support insole on people with flatfoot during uphill and downhill walking. In: 34th International Conference on Biomechanics in Sports; 18-22 July, 2016; Tsukuba, Japan: International society for biomechanics in sports; 2016. p. 275-8.

[3] Kang LP, Gong TS. Design of 3D printed pressure-reducing insoles based on changes in parameters of lattice structure. Advances in Mechanical Engineering. 2023; 15(12):1-11 https://doi.org/10.1177/16878132231216609

[4] Huang Y, Kim K, Song CY, Chen YH, Peng HT. How arch support insoles help persons with flatfoot on uphill and downhill walking. Journal of Healthcare Engineering. 2017; 2017:1-6. https://doi. org/10.1155/2017/9342789

[5] Endo Y, Kanai Y, Yozu A, Kobayashi Y, Fukaya T, Mutsuzaki H. Influence of a foot insole for a down syndrome patient with a flat foot: A case study. Medicina. 2020; 56(5). https://doi. org/10.3390/medicina56050219

[6] Jonnala UK, Sankineni R, Ravi KY. Design and development of fused deposition modeling (FDM) 3D-printed orthotic Insole by using gyroid structure. Journal of the Mechanical Behavior of Biomedical Materials. 2023; 145:106005. https://doi.org/10.1016/j.jmbbm.2023.106005

[7] Davia-Aracil M, Hinojo-Pérez JJ, Jimeno-Morenilla A, Mora-Mora H. 3D printing of functional anatomical insoles. Computers in Industry. 2018; 95:38-53. https://doi.org/ 10.1016/j.compind.2017.12.001

[8] Wang JC, Dommati H, Cheng J. A Turnkey Manufacturing Solution for Customized Insoles Using Material Extrusion Process. In: Kumar LJ, Pandey PM, Wimpenny DI, editors. 3D Printing and Additive Manufacturing Technologies. Singapore: Springer Singapore; 2019. p. 203-16. https://doi.org/10.1007/978-981-13-0305-0_18

[9] Terry S, Tantawi K. Preliminary investigation into metal-material extrusion. Progress in Additive Manufacturing. 2021; 6: 133-141. https://doi.org/10.1007/s40964-020-00151-5

[10] Manmadhachary A, Ravi KY, Krishnanand L. Improve the accuracy, surface smoothing and material adaption in STL file for RP medical models. Journal of Manufacturing Processes. 2016; 21:46-55. https://doi.org/10.1016/j.jmapro.2015.11.006

[11] Rahmatabadi D, Aminzadeh A, Aberoumand M, Moradi M. Mechanical characterization of fused deposition modeling (FDM) 3D printed parts. In: Dave HK, Davim JP, editors. Fused Deposition Modeling Based 3D Printing. Cham: Springer International Publishing; 2021. p. 131-50. https://doi.org/10.1007/978-3-030-68024-4_7

[12] Mogan Y, Sa'aban N, Ibrahim M, Periyasamy R. Thermoplastic elastomer infill pattern impact on mechanical properties 3D printed customized orthotic insole ARPN Journal of Engineering and Applied Sciences. 2016; 11(10):6519-6524.

[13] Daryabor A, Kobayashi T, Saeedi H, Lyons SM, Maeda N, Naimi SS. Effect of 3D printed insoles for people with flatfeet: A systematic review. Assistive Technology. 2023; 35(2):169-79. https://doi.org/10.1080/10400435.2022.2105438

[14] Ali MH, Trubayev S, Shehab E, editors. 3D printed large-scale insole and its printing challenges. 8th Brunei International Conference on Engineering and Technology; 23-25 October 2023; Darussalam, Brunei: AIP Conference Proceedings. https://doi.org/10.1063/5.0110272

[15] Orsu B, Shaik YP. Compression strength analysis of customized shoe insole with different infill patterns using 3D printing. Open Access Library Journal. 2022; 9:1-13. https://doi.org/10.4236/oalib.1108712

[16] Tanveer M, Mishra G, Mishra S, Sharma R. Effect of infill pattern and infill density on mechanical behaviour of FDM 3D printed Parts- a current review. Materials Today: Proceedings. 2022; 62:100-108. https://doi.org/10.1016/j.matpr.2022.02.310

[17] Favero CS, English JD, Cozad BE, Wirthlin JO, Short MM, Kasper FK. Effect of print layer height and printer type on the accuracy of 3-dimensional printed orthodontic models. American Journal of Orthodontics and Dentofacial Orthopedics. 2017; 152(4):557-65. https://doi.org/10.1016/j.ajodo.2017.06.012

[18] Simarmata TP, Martawidjaja M, Harito C, Tobing CCL. Three-Dimensional Printed Auxetic Insole Orthotics for Flat Foot Patients with Quality Function Development/Theory of Inventive Problem Solving/Analytical Hierarchy Process Methods. Designs. 2025; 9(1):15. https://doi.org/10.3390/designs9010015

[19] Cracknell D, Battley M, Fernandez J, Amirpour M. The mechanical response of polymeric gyroid structures in an optimised orthotic insole. Biomechanics and modeling in mechanobiology. 2025; 24(1):311-29. https://doi.org/10.1007/s10237-024-01912-9

[20] Phitsjax. phitsjax [Internet]: phitsjax.com. 2020. [cited 2024]. Available from: https://phitsjax.com/rs-scan/

[21] Yick KL, Tse CY. 17 - Textiles and other materials for orthopaedic footwear insoles A2 - Luximon, A. Handbook of Footwear Design and Manufacture: Woodhead Publishing; 2013. p. 341-71. http://dx.doi.org/10.1533/9780857098795.4.341

[22] Tlegenov Y, Hong GS, Lu WF. Nozzle condition monitoring in 3D printing. Robotics and Computer-Integrated Manufacturing. 2018;54:45-55. https://doi.org/10.1016/j.rcim.2018.05.010

[23] Hentschel T, Münstedt H. Thermoplastic polyurethane—The material used for the erlanger silver catheter. Infection. 1999; 27(1):S43-S5. https://doi.org/10.1007/BF02561617

[24] Gleadall A. FullControl GCode Designer: Open-source software for unconstrained design inadditive manufacturing. Additive Manufacturing. 2021; 46:102-109. https://doi.org/10.1016/j.addma.2021.102109

[25] Hsu CY, Wang CS, Lin KW, Chien MJ, Wei SH, Chen CS. Biomechanical analysis of the flatfoot with different 3D-printed insoles on the lower extremities. Bioengineering. 2022; 9(10):1-12. https://doi.org/10.3390/bioengineering9100563

[26] Naramore C. 3D printing [Internet]: 3dprinting.com. 2020. [cited 2025]. Available from: https://3dprinting.com/how-to/tutorial-3d-printing-reusable-tpu-molds-for-epoxy-resin/

[27] O'Connell J. Printing atoms [Internet]: printingatoms.com. 2022. [cited 2025]. Available from: https://printingatoms.com/3d-print-layer-height/

[28] Ayrilmis N. Effect of layer thickness on surface properties of 3D printed materials produced from wood flour/PLA filament. Polymer Testing. 2018;71:163-166. https://doi.org/10.1016/j.polymertesting.2018.09.009

[29] National Standard. GBT 3903.1-2017 Test method for whole shoe durability 2017. Available from: https://www.doc88.com/p-0933884711765.html

[30] National Standard NS. (HG_T 2876-2009 Test Method for Compression Deformation of Microporous Materials in Rubber Shoes) HG_T 2876-2009. 2009. Available from: https://www.doc88.com/p-7038457519540.html

[31] Gómez-Castañeda M, Cuan-Urquizo E, Giraldo-Betancur A, Félix-Martínez C, Gómez-Ortega A, Alvarado-Orozco J. Additive manufacturing and mechanical characterization of sinusoidal-based lattice structures: A numerical and experimental approach. Progress in Additive Manufacturing. 2024; 9(2):315-30. https://doi.org/10.1007/s40964-023-00453-4

[32] Kilian D, Holtzhausen S, Groh W, Sembdner P, Czichy C, Lode A, et al. 3D extrusion printing of density gradients by variation of sinusoidal printing paths for tissue engineering and beyond. Acta Biomaterialia. 2023; 158:308-23. https://doi.org/10.1016/j.actbio.2022.12.038